Manuscript prepared for J. Name
with version 5.0 of the LaTeX class copernicus.cls.
Date: 21 April 2015

C.Lang x.Fettweis M.Erpicum

Future climate and surface mass balance of Svalbard glaciers in an RCP8.5 climate scenario: a study with the regional climate model MAR forced by MIROC5

Département de Géographie, Université de Liège, Liège, Belgium

Correspondence to: C. Lang (charlotte.lang@ulg.ac.be)

Abstract. We have performed a future projection of the climate and surface mass balance (SMB) of Svalbard with the MAR regional climate model forced by the MIROC5 global model, following the RCP8.5 scenario at a spatial resolution of 10 km. MAR predicts a similar evolution of increasing surface melt everywhere in Svalbard followed by a sudden acceleration of the melt around 2050, with a larger melt increase in the south compared to the north of the archipelago. This melt acceleration around 2050 is mainly driven by the albedo-melt feedback associated with the expansion of the ablation/bare ice zone. This effect is dampened in part as the solar radiation itself is projected to decrease due to cloudiness increase. The near-surface temperature is projected to increase more in winter than in summer as the temperature is already close to 0 °C in summer. The model also projects a stronger winter west-to-east temperature gradient, related to the large decrease of sea ice cover around Svalbard. By 2085, SMB is projected to become negative over all of Svalbard's glaciated regions, leading to rapid degradation of the firn layer.

1 Introduction

Worldwide, glaciers and ice caps are observed to retreat. At present, they contribute to sea level rise (SLR) as much as the Antarctic and Greenland ice sheets (Gardner et al., 2013; Shepherd et al., 2012). Arctic glaciers have been the second contributor to SLR among glaciers and ice caps between 1961 and 2004 (Kaser et al., 2006). However, contrary to what was previously estimated (Meier et al., 2007; Meehl et al., 2007), glaciers and ice caps (as found over Svalbard for example) are no longer believed to be the dominant contributors to SLR in the next decades, as the melt of the Antarctic and Greenland ice sheets has been accelerating (Rignot et al., 2011, 2014). Yet, the vanishing of Svalbard glaciers could have huge impacts on the fauna and flora, permafrost (Isaksen et al., 2007; Etzelmüller et al., 2011), tourism and even possibly the development of agriculture. Future projections of the Svalbard climate have been made (Førland et al., 2011) but the future evolution of the glaciers of Svalbard themselves have been little studied and most studies focussed on past and present surface mass balance (Lang et al. (2015) and references therein). Day et al. (2012) have studied the impact of the future sea ice decline on the temperature, precipitation and surface mass balance (SMB) of Svalbard while Radić and Hock (2011), Marzeion et al. (2012) and Radić et al. (2014) have evaluated the contribution of Svalbard glaciers to future sea level rise. These SMB calculations are based on empirical models and are rarely forced by outputs from high resolution atmospheric models but rather by global ones. Therefore, we propose a more extensive study at high resolution (10km) of the future of Svalbard glaciers and ice caps using the regional climate model MAR (Modèle Atmosphérique Régional) evaluated over the current Svalbard climate in the companion paper Lang et al. (2015). For the first time, this study uses an atmospheric model fully coupled to a snow module, explicitly solving the energy and mass balance of glaciated regions. This coupling allows to explicitly take into account the atmosphere-surface feedbacks in future SMB projections. This computationally intensive approach currently allows only a single scenario and forcing model to be used, but we provide evidence in Sect. 2 that this is a representative combination of models. In Sect. 3, we present the future SMB of Svalbard and its regional evolution through the 21st century. In Sect. 4, we investigate the temperature change and how it should be impacted by the sea ice cover decrease. In Sect. 5, we describe the evolution of the melt season and, finally, the sensitivity of the energy balance

components to rising temperatures is investigated in Sect. 6 before concluding in Sect. 7.

2 Models and climate forcings

MAR (Gallée and Schayes, 1994) is a regional climate atmospheric model fully coupled to a surface model resolving the energy balance at the surface of the snow pack and has been described in Lang et al. (2015). The version and forcings of the model are the same as those used over the present era in Lang et al. (2015). We have run MAR over the period 2006–2100 at a spatial resolution of $10\,\mathrm{km}$. The lateral and upper (tropopause) boundaries (temperature, humidity, wind speed and surface pressure) as well as oceanic boundaries (sea surface temperature and sea ice cover) were forced every $6\,\mathrm{h}$ by the MIROC5 (Model for Interdisciplinary Research on Climate) global model (Watanabe et al., 2010; Sakamoto et al., 2012) using the RCP8.5 scenario (Moss et al., 2010).

MIROC5 has been successfully evaluated over Svalbard in the companion paper Lang et al. (2015). MIROC5 performs as one of the best CMIP5 GCMs over Greenland (Fettweis et al., 2013; Belleflamme et al., 2012). Over Svalbard, MIROC5 also performs well and the near-surface temperature bias from MIROC5 is no longer significant over land in MAR forced by MIROC5. As a result, SMB, precipitation and runoff modelled by MAR forced by ERA-Interim and MRIOC5 are not significantly different over the present era.

Melt increases non-linearly with temperature, so it is very important to realistically simulate the present climate, especially the elevation of the $0\,^{\circ}\mathrm{C}$ isotherm. Of course, simulating a realistic current climate does not necessarily mean that future changes are also robust. CMIP5 GCMs do not project significant circulation changes in the Arctic (Belleflamme et al., 2012) so that projected temperature changes dominate the SMB change (Fettweis et al., 2013). The temperature increase projected by MIROC5 follows the CMIP5 ensemble mean until 2060 (Fig. 1) and exceeds the ensemble mean after that. Our projection for 2100 with this forcing may therefore be representative for later decades, not altering the main results. The extreme scenario RCP8.5 has been chosen to have a forced warming signal that significantly exceeds natural interannual variability.

3 Surface mass balance

Figure 2a shows that MAR SMB is projected to be negative on average over 2070–2099 over the entire archipelago, according to the MIROC5-based RCP8.5 scenario. $\mathrm{MAR}_{\mathrm{RCP8.5}}$ predicts that the greatest losses will mostly happen in the southern part of Spitsbergen with values lower than $-4000\,\mathrm{mm\,w.e.\,yr^{-1}}$ in the most extreme cases, where we also have the largest differences compared to the 1980–2005 average (Fig. 2b and Fig. 14 in Lang et al. (2015) ($\mathrm{MAR}_{\mathrm{histo}}$)). This suggests that the surface mass loss from small southern glaciers will be higher than over the ice caps and large ice fields of northern Spitsbergen. The mean 2070–2099 meltwater runoff anomaly is largely positive (Fig. 2c) and the largest anomalies ($> 5000\,\mathrm{mm\,w.e.\,yr^{-1}}$) are also located in the south of the archipelago. The snowfall will mostly increase (Fig. 2d) but far from enough to compensate for the increase in meltwater runoff, as also simulated by MAR over the Greenland ice sheet (Fettweis et al., 2013) and by RACMO2 in the Canadian Arctic Archipelago (Lenaerts et al., 2013). At lower elevations however, the snowfall anomaly is mostly negative, because the winter solid precipitation increase will not be able to compensate for the summer decrease, as a large part of the current snowfall is projected to become rainfall at the end of this century.

Figure 3, showing the temporal evolution of the annual SMB for five different regions around the archipelago, confirms that the surface mass loss acceleration after 2050 is larger in the south of the archipelago than in the north. $\mathrm{MAR}_{\mathrm{histo}}$ and $\mathrm{MAR}_{\mathrm{RCP8.5}}$ project a similar SMB evolution for all our 5 regions until 2050. After 2050, the acceleration of surface mass loss is projected to increase suddenly and be more pronounced in the south of Spitsbergen and on Barentsøya and Edgeøya (BE) than in west/east Spitsbergen and on Austfonna and Vestfonna (AV). After 2085, the surface mass loss is projected to stabilize and even to increase slightly according to the MIROC5-based RCP85 scenario. The SMB future evolution is primarily determined by the significant runoff increase (Fig. 4a), as the snowfall remains much more constant in time and very similar from region to region (Fig. S1a).

The increasing summer near-surface temperature ($\mathrm{TAS}_{\mathrm{JJA}}$, JJA for June-July-August) explains in part the acceleration of the melt around 2050 but not the regional differences (Fig. 4b), resulting rather from the surface JJA albedo-melt feedback (Fig. 4c) associated with the expansion of the ablation/bare ice zone as also projected over the Greenland ice sheet (Franco et al., 2013). However, the melt-JJA albedo feedback is partly reduced in the west by the decrease of the solar flux at the surface caused by a larger cloud optical depth in west and south Spitsbergen in summer, compared to the northeast and the AV ice caps (Fig. S1b and c). The larger cloud optical depth in the west and the south is caused by a warmer and therefore more humid atmosphere. As a result, despite a larger decrease of JJA surface albedo in west Spitsbergen than in the other northern regions, the amount of net shortwave radiation absorbed by the surface in west Spitsbergen is closer to the amount over the other regions (Fig. 4d).

Figure 5 shows the projected yearly anomaly (with respect to the historical mean) of the SMB integrated over the 21st century. This gives an estimation of the impact on the ice caps topography of the SMB changes integrated over this century (by assuming that there is no change in ice dynamics). In the south and along the west coast, some glaciers could lose more than $200\,\mathrm{m\,w.e.}$ over the 21st century. BE is projected to be the first of our five regions to undergo net ablation as

$MAR_{RCP8.5}$ projects that the accumulation zone on BE is projected to disappear by 2065 and will be reduced to less than 5% of the total glaciated area of BE as soon as 2035 (Fig. 6). In south Spitsbergen, the vanishing of the accumulation zone is projected to happen around 2065 and even Austfonna and Vestfonna will undergo net ablation at the end of the 21st century, leading to rapid degradation of firn. However, on Austfonna, given the large ice thickness (Dowdeswell et al., 2008), we expect that a great part (in area) of the ice cap will still remain at the end of the century even if the SMB is negative everywhere and that the retreat will only concern the margins in 2100.

Over the whole 21st century, the integrated Svalbard $MAR_{RCP8.5}$-based SMB decrease corresponds to a mass loss of $-2600\,\mathrm{km^3\,w.e.}$ (i.e. $-2827\,\mathrm{km^3}$ of ice) with respect to the historical mean. The $MAR_{RCP8.5}$ SMB decrease compared to the present value is therefore projected to contribute $7.2\,\mathrm{mm}$ to the 21st century sea level rise (SLR), according to MIROC5-based $MAR_{RCP8.5}$. Radić et al. (2014) calculated a mean value of the sea level rise associated with the 21st century SMB changes of Svalbard with a Positive Degree-Day (PDD) model based on the outputs of an ensemble of 14 GCMs for the RCP8.5 scenario. Their projected SLR at the end of the century is more than twice as large as ours ($15.81\,\mathrm{mm}$). Marzeion et al. (2012) projected a SLR between 15 and $25\,\mathrm{mm}$ for Svalbard for the RCP8.5 scenario, with an empirical model based on the outputs of climatologies and CMIP5 GCMs. However, these values were based on large scale temperature and precipitation changes from global models in most of which the topography of Svalbard is not explicitly represented given their huge spatial resolution. Moreover, the surface temperature of glaciated regions is limited to $0\,^\circ\mathrm{C}$ in MAR, damping the MAR near-surface temperature increase (Fig. 1), whereas there is no limitation in most GCMs (Goelze et al., 2013). Then, those studies are based on empirical calculations of the energy balance while ours are physically based, which also explains part of the the differences in SMB values. Finally, there is also an error in our estimation due to the use of a fixed ice mask and topography. However, we estimate this error to be small (10 % of the SMB anomaly, see discussion below) and the SLR contribution from MAR would still have been twice as small as Marzeion et al. (2012) and Radić et al. (2014) estimation if we had not used a fixed ice mask and topography.

Radić et al. (2014) estimated the total present ice volume of Svalbard to be $9089\,\mathrm{km^3}$, which corresponds to a potential sea level rise of $23\,\mathrm{mm}$. Our projection therefore suggests that 31 % of their present estimated volume will disappear by 2100. According to a previous estimate of $7000\,\mathrm{km^3}$ (equivalent to a sea level rise of $20\,\mathrm{mm}$) by Hagen et al. (1993), about 40 % of the ice mass is projected to disappear by 2100 in our projection, due to surface mass loss only.

As shown in Lang et al. (2015), a resolution of $10\,\mathrm{km}$ smoothens the topography, especially on Spitsbergen where the topography is very steep. As a result, the elevation is underestimated over a large part of Svalbard and some low altitude glaciers should not even exist in our $10\,\mathrm{km}$ grid, causing a likely overestimation of the surface mass loss in our projection. Moreover, glaciers are typically concentrated at higher elevations, where the negative elevation bias in MAR is largest, leading to further overestimated mass loss. The topography is also fixed in our simulations, which is an acceptable approximation under the present climate but will likely introduce an underestimation of the melt increase in the future, as a result of surface lowering. On the other hand, glaciers are going to retreat in the future and using a fixed ice mask like we do overestimates the melt, as some areas should not be covered with permanent ice under the future warmer climate. The contribution of these areas (with relatively high mass loss) to the sea level rise should be removed in our projection. As the aforementioned effects partly compensate each other we expect a relatively minor impact on our future projection. According to Goelze et al. (2013), the additional SMB changes coming from topography changes are about 10 times lower than SMB changes directly induced by climate warming. Over the Greenland ice sheet, those effects are projected to contribute to about only 5–10 % of the SMB anomaly by the end of the century (Fettweis et al., 2013) and we assume their contribution to be of the same order of magnitude in Svalbard. However, only a high resolution simulation coupled with an ice sheet model could yield insight in the magnitude of this contribution. In southern Spitsbergen, given the very negative values of SMB and the fact that glaciers rather than ice caps prevail, we expect the retreat effect to be dominant and $MAR_{RCP8.5}$ probably overestimates the surface mass loss in this area. On Austfonna, on the other hand, we expect the retreat to be limited only to the proximity of the margins but the elevation decrease towards the centre of the ice cap is also expected to be limited. We therefore expect that, on Austfonna, both effects will balance each other, or at least that none of them will be largely dominant.

4 Near-surface temperature

$MAR_{RCP8.5}$ predicts a rather small near-surface temperature increase in summer (TAS_{JJA} increase of 3.0 to $6.5\,^\circ\mathrm{C}$) compared to the winter increase (TAS_{DJF} (December-January-February) increase of 11 to $25\,^\circ\mathrm{C}$) (Figs. 7c, 7d and 9a). The spatial range of temperature increase over our domain is also much smaller in summer than in winter ($3\,^\circ\mathrm{C}$ vs almost $15\,^\circ\mathrm{C}$), due to the presence of a 10-degree west-to-east winter gradient projected by MAR.

The pattern and magnitude of the temperature increase modelled by $MAR_{RCP8.5}$ are similar to Day et al. (2012) estimates. Førland et al. (2011) projected a temperature increase in Longyearbyen of 2.8 and $10.4\,^\circ\mathrm{C}$ in JJA and DJF by the end of the century using B2, A1B and A2 scenarios while our temperature is projected to increase by $6\,^\circ\mathrm{C}$ in JJA and $14\,^\circ\mathrm{C}$ in DJF. Considering that Day et al. (2012) and Førland et al.

(2011) worked with B2, A1B and A2 scenarios and we used RCP8.5, it is expected that our temperature increase is larger (Rogelj et al., 2012) and we can conclude that our results are in qualitative agreement with those of Day et al. (2012) and Førland et al. (2011).

In summer, TAS is already close to $0\,^{\circ}\mathrm{C}$ over the historical period (Fig. 7a) and can not increase very much because the excess energy available at the surface is used to melt snow/ice. According to our MIROC5-based RCP8.5 scenario, JJA temperature is projected to increase by 3.75 to $4.75\,^{\circ}\mathrm{C}$ over the glaciated areas (Fig. 7c) and the only regions where the TAS increase is larger (up to $6.5\,^{\circ}\mathrm{C}$) are regions with small permanent ice area at present, i.e. BE and Nordenskiöld Land (orange/red area separating the north and south of Svalbard in Fig. 7c).

The higher temperature increase in winter is due to (i) very low present-day DJF temperatures (Fig. 7b) allowing it to increase much more before reaching freezing point and (ii) the projected decrease of the winter sea ice cover (SIC) (also highlighted by Day et al., 2012 and Førland et al., 2011), that is also responsible for the large west-to-east temperature gradient. At present, there is a large west-to-east SIC gradient, caused by the North Atlantic Drift that prevents sea ice to form west of Svalbard. In a warming climate, the SIC gradient will decrease, hence strongly reducing the west-to-east gradient in near-surface air temperature.

In the future, near-surface temperature will increase more in areas where sea ice can decrease. Therefore, in the west, as there is already no significant sea ice cover in the present climate, the projected increase is much lower than in the east. We have shown in Lang et al. (2015) that the ocean has a large influence on the climate in Svalbard, even quite far inland. In Fig. 7a, showing the 1980–2005 mean JJA TAS, the temperature follows the topography whereas in winter (Fig. 7b), the most dominent temperature gradient is the west-to-east gradient due to the presence or absence of sea ice. At the end of the century, the effect of topography is projected to become dominant in winter (Fig. S2b) as most of the sea ice will have disappeared according to the MIROC5-based RCP8.5 scenario. The DJF east coast maximum temperature increase in Day et al. (2012) is located on the east coast of Nordaustlandet whereas ours is on BE and our Nordaustlandet anomaly rather lies around $+16/17\,^{\circ}\mathrm{C}$, compared to $+21\,^{\circ}\mathrm{C}$ in Day et al. (2012) using HadRM3. This is probably due to the fact that MIROC5 overestimates the present sea ice extent and still has up to $40\,\%$ of sea ice cover on the east coast of Nordaustlandet over the period 2070–2099 (Fig. S3) whereas HadGEM1 (used as forcings in Day et al. (2012)) ocean is mostly ice-free at the end of this century.

5 Melt season

During the first half of this century, $\mathrm{MAR}_{\mathrm{RCP8.5}}$ projects that the beginning of the melt season (Fig. 8a) will not vary much (melt season will start 0.2 day earlier per year) because the effect of the temperature increase bringing more energy for the melt (Fig. 9a) will be compensated by the albedo effect (Fig. 9c) induced by increasing winter snowfall (Fig. 9b). As the amount of snowfall increases, so does the winter snowpack height above bare ice/old dirty snow at the beginning of the summer. The appearance of low albedo zones in summer is therefore delayed and SWnet available for the melt in the energy budget is reduced. After the 2050s, the temperature increase is projected to dominate the effect of heavier snowfall accumulation and the melt season is expected to start significantly sooner (1.5 day earlier per year).

The seasonal maximum of melt happens around 15–20 July through the whole 21st century and coincides with the temperature maximum. Before 2050, the temperature seasonal cycle is more or less symmetrical with respect to its maximum value. The melt (resp. albedo) seasonal cycle is also symmetrical with respect to its maximum (resp. minimum) (Figs. 8b and 9c). In the second half of the century, the temperature and therefore the melt are projected to increase more after their seasonal maximum than at the beginning of summer. The melt asymmetry is also partly explained by changing snowfall that is projected to increase before June but to significantly decrease in late summer, impacting the melt through the positive albedo feedback.

As soon as the 2030s, the $\mathrm{MAR}_{\mathrm{RCP8.5}}$ time of runoff maximum coincides with the time of melt maximum (Fig. 8d, e and f). The 5 to 8 day delay visible on Fig. 8d, e and f corresponds to the time needed in MAR for the meltwater to runoff from the glaciers to the sea as parametrized in Zuo and Oerlemans (1996). The maximum of runoff is also projected to be equal (or almost) to the maximum of melt. This concordance in time is due to the fact that, from the 2030s, at the time of the maximum of melt, a smaller fraction of the melting area is covered with snow (retaining part of the meltwater and delaying the runoff) and large areas are covered with bare ice or impermeable snowpack (snow becomes impermeable when its density reaches 830 $\mathrm{kg\,m^{-3}}$ and prevents meltwater to percolate and refreeze) damping the meltwater retention capacity of the glaciers. During the historical period and until the 2020s on the other hand, the presence of snow above ice in the ablation zone allows part of meltwater to be stored in the snowpack and refreeze in winter without running off. van Angelen et al. (2013) also projected a rapid decrease of the refreezing capacity of the Greenland ice sheet and its buffering role in the future. Conversely, at the beginning of the melt season, there is still a small delay between the melt and runoff seasons as the bare ice is covered by the winter snowpack even at the end of the century. However, this delay will decrease steadily with time, as the water storage and refreezing capacity will also decrease, as

a consequence of the snow cover decrease in the enlarging ablation zone.

6 Energy balance

Studying energy balance components anomaly vs. temperature anomaly (rather than vs. time) offers the advantage that results do not depend on the choice of a particular future scenario, as shown by Fettweis et al. (2013).

The net energy available at the surface for the melt (NET) can be calculated as follows:

$$\mathrm{NET} = \mathrm{SWnet} + \mathrm{LWnet} + \mathrm{SHF} + \mathrm{LHF} \quad (\mathrm{W\,m^{-2}}) \qquad (1)$$

where

- $\mathrm{SWnet} = \mathrm{SWD} \times (1 - a)$ is the net shortwave radiation, i.e. the amount of the downward shortwave (= solar radiation) energy flux (SWD) that is absorbed by the surface following its albedo (a).
- $\mathrm{LWnet} = \mathrm{LWD} - \mathrm{LWU}$ is the net longwave radiation, i.e., the difference between the downward longwave radiation coming from the atmosphere and the upward longwave radiation emitted by the surface.
- SHF and LHF are the sensible and latent heat fluxes.

In summer, the snowpack is melting and the subsurface heat flux is therefore negligible. In the future, it will become even more negligible as larger and larger parts of the glaciated area will start melting and most of the snowpack will have a temperature of $0\,^{\circ}\mathrm{C}$. We therefore do not take this flux into account in the energy balance equation.

Figure 10b shows that the JJA net energy flux at the surface (and therefore melt and runoff, Fig. 10a) quadratically increase with the JJA TAS projected changes, as also projected over Greenland (Franco et al., 2013). Figure 10c shows the evolution of the anomaly of each energy balance component (JJA) as a function of the $\mathrm{TAS_{JJA}}$ anomaly. In order to distinguish the albedo and solar radiation effects in SWnet, we have estimated two additional variables for the net solar radiation, as done in Franco et al. (2013). First, we computed SWDswd by using the 1980 to 2099 SWD outputs and the 1980–2005 mean value of the surface albedo. Secondly, we computed SWDalb by using the 1980 to 2099 albedo outputs and the 1980–2005 mean value of SWD.

$\mathrm{MAR_{RCP8.5}}$ predicts that, at the end of the century (2080–2099 mean), the anomaly of SWnet will represent 33 % of the NET anomaly while the SWDalb anomaly, reflecting the effect of the albedo on SWnet, will count for 50 % of the NET anomaly (Table 1). The expected increase in cloud optical depth will decrease the incident solar radiation at the surface (SWDswd, Fig. 10c) and partly compensates for the increase of SWDalb associated with the decreasing albedo, leading to a positive and increasing SWnet, as also projected over Greenland (Franco et al., 2013).

The second contribution to the NET increase is the sensible heat flux, whose anomaly at the end of the century is projected to represent 24 % of the NET anomaly, as a consequence of the advection of warmer (oceanic) air over the cold ice/snow surface. At present, the modelled TAS is negative on average in summer and therefore lower than the snow/ice temperature ($0\,^{\circ}\mathrm{C}$ as the surface snow/ice is melting). SHF is thus also negative and the surface loses energy to the atmosphere. $\mathrm{MAR_{RCP8.5}}$ predicts that, around 2030, the summer near-surface temperature will become positive and consequently higher than the melting snow/ice temperature. The JJA SHF averaged over the entire Svalbard will also become positive.

The third contribution to the NET change is the latent heat flux, counting for 22 % over Svalbard, whereas it is the smallest contributor of the energy fluxes over Greenland (Franco et al., 2013). LHF is currently negative as evaporation and sublimation, requiring energy, are the dominant processes but they will decrease in the future in favour of condensation and deposition (giving energy to the surface) as more and more humid and warm air due to the reduction of sea ice during summer will be advected towards the cold ice surface. On the other hand, condensation and deposition will also directly contribute to accumulation (10 % of the mean 2080–2099 accumulation) and act to oppose mass loss. In contrast to the Greenland ice sheet (Noël et al., 2014), which is higher in altitude, the oceanic conditions around Svalbard have a large impact on its climate. In Svalbard, the katabatic winds, weaker than in Greenland, can not prevent the warm oceanic air to penetrate up to the central regions and the SHF and LHF increase will take place over the entire land area instead of along the ice sheet margins as in Greenland (Franco et al., 2013).

Finally, the weakest contribution will come from the net longwave radiation flux (LWnet, 21 % of the 2080–2099 NET anomaly). The increase in longwave radiation emitted downward by the warmer and wetter atmosphere following the increase of the greenhouse gases concentration will partly be counterbalanced by the increase in upward longwave radiation emitted by the surface, due to the surface temperature increase.

7 Conclusions

Over the 21st century, according to $\mathrm{MAR_{RCP8.5}}$, the warming induced SMB decrease will be amplified by the snow/ice albedo feedback related to the extension of the ablation area that will increase the net shortwave radiation absorbed by the surface (and thus increase the energy available for the melt) and will decrease the meltwater retention capacity. The projected rapid decrease of the albedo will cause an acceleration of the mass loss around 2050. $\mathrm{MAR_{RCP8.5}}$ simulates a larger acceleration of the mass loss in the south of the archipelago compared to the north. This regional difference

is due to a larger increase of JJA SWnet in the south, related to the larger decrease of the JJA surface albedo. SWnet is the component of the energy balance the most sensitive to an increase in temperature because of the decreasing surface albedo. However, the downward shortwave radiation itself also decreases with increasing temperature due to an increase in cloud optical depth which partly counterbalance the effect of the melt-albedo positive feedback.

The summer sensible and latent heat fluxes are both negative at present but will increase with increasing temperature and become positive in the future thereby heating the surface. The LHF increase will be caused by the decreasing SIC allowing more evaporation around Svalbard and warmer and more humid air to be advected over the cold ice surface, showing the significant impact of the oceanic conditions on Svalbard, even far inland. The SHF will become positive when the temperature of the warmer oceanic air advected over the cold ice/snow surface will become positive, causing the atmosphere to give energy to the surface.

The temperature is projected to increase more in winter than in summer as (i) the surface temperature is limited to $0\,^{\circ}\mathrm{C}$, damping the temperature increase in summer and (ii) sea ice retreat is higher in winter than in summer since a large part of the ocean surrounding Svalbard is already ice free in the current climate (Day et al. (2012) and Førland et al. (2011)). Because of the larger present sea-ice cover east of the archipelago than west of it, the winter temperature increase will be larger in the east than in the west.

All glaciated areas of the archipelago are projected to undergo net ablation by the end of the century. The disappearance of the accumulation zone is projected to happen much earlier in the south and northwest of Spitsbergen than in the northeast and on the ice caps. But, even in these regions, the accumulation area is projected to completely disappear by the end of the century. The contribution of Svalbard 21st century SMB changes to sea level rise under the RCP8.5 scenario will be about $7.1\,\mathrm{mm}$, according to MIROC5-forced MAR.

The increase of snowfall accumulation during winter and spring and the small increase in temperature at the beginning of the melt season explain why, during the first half of this century, the melt season is not expected to start much earlier than now, as the low albedo zones will be covered by a thicker winter snowpack. However, as the melt area is projected to be no longer covered with melting snow but rather with bare ice at the time of the maximum of melt as soon as the 2030s, the meltwater retention and refreezing capacity of the ice sheet will decrease a lot and the maximum of runoff will be equal to the maximum of melt and there will not be any delay between them quite rapidly.

Finally, it should be noted that the ice caps topography is fixed during our simulation, suggesting that we underestimate the surface mass loss in our projection as glacier thinning is not taken into account. On the other hand, our ice sheet mask is also fixed, suggesting that our projected integrated surface melt includes ice areas that will disappear in the near future and therefore that we overestimate the contribution of Svalbard to the sea level rise. This motivates the necessity to couple MAR with an ice sheet model in further developments to evaluate if not taking into account the glaciers thinning is counterbalanced by the use of a fixed permanent ice mask or not. In addition, a 10km resolution results in an underestimation of the topography over most of the achipelago and an increased melt. Future projections at higher resolution ($\sim 5\,\mathrm{km}$) are therefore required to better resolve the altitude of small glaciers.

Supplementary material related to this article is available online at: http://\@journalurl/\@pvol/\@fpage/\@pyear/\@journalnameshortlower-\@pvol-\@fpage-\@pyear-supplement.pdf.

Acknowledgements. C. Lang works under a PhD grant from the Fonds pour la formation à la Recherche dans l'Industrie et l'Agriculture (FRIA), Belgium. The authors wish to thank two anonymous reviewers, Marco Möller and Michiel van den Broeke, whose comments helped improve this manuscript a lot.

References

references

Belleflamme, A., Fettweis, X., Lang, C., and Erpicum, M.: Current and future atmospheric circulation at 500 hPa over Greenland simulated by the CMIP3 and CMIP5 global models, Clim. Dynam., 4, 2061–2080, doi:10.1007/s00382-012-1538-2, 2012.

Day, J. J., Bamber, J. L., Valdes, P. J., and Kohler, J.: The impact of a seasonally ice free Arctic Ocean on the temperature, precipitation and surface mass balance of Svalbard, The Cryosphere, 6, 35–50, doi:http://dx.doi.org/10.5194/tc-6-35-201210.5194/tc-6-35-2012, 2012.

Dowdeswell, J. A., Benham, T. J., Strozzi, T., and Hagen, J. O.: Iceberg calving flux and mass balance of the Austfonna ice cap on Nordaustlandet, Svalbard, J. Geophys. Res., 113, F03022, doi:http://dx.doi.org/10.1029/2007JF00090510.1029/2007JF000905, 2008.

Etzelmüller, B., Schuler, T. V., Isaksen, K., Christiansen, H. H., Farbrot, H., and Benestad, R.: Modeling the temperature evolution of Svalbard permafrost during the 20th and 21st century, The Cryosphere, 5, 67–79, doi:http://dx.doi.org/10.5194/tc-5-67-201110.5194/tc-5-67-2011, 2011.

Fettweis, X., Franco, B., Tedesco, M., van Angelen, J. H., Lenaerts, J. T. M., van den Broeke, M. R., and Gallée, H.: Estimating the Greenland ice sheet surface mass balance contribution to future sea level rise using the regional atmospheric climate model MAR, The Cryosphere, 7, 469–489, doi:http://dx.doi.org/10.5194/tc-7-469-201310.5194/tc-7-469-2013, 2013.

Førland, E. J., Benestad, R., Hanssen-Bauer, I., Haugen, J. E., and Skaugen, T. E. : Temperature and precipitation development at Svalbard 1900–2100, Adv. Meteorol., 2011, 893790, doi:http://dx.doi.org/10.1155/2011/89379010.1155/2011/893790, 2011.

Franco, B., Fettweis, X., and Erpicum, M.: Future projections of the Greenland ice sheet energy balance driving the surface melt, The Cryosphere, 7, 1–18, doi:http://dx.doi.org/10.5194/tc-7-1-201310.5194/tc-7-1-2013, 2013.

Gallée, H., and Schayes, G.: Development of a three-dimensional meso-γ primitive equation model: katabatic winds simulation in the area of Terra Nova Bay, Antarctica, Mon. Weather Rev., 122, 671–685, 1994.

Gardner, A. S., Moholdt, G., Cogley, J. G., Wouters, B., Arendt, A. A., Wahr, J., Berthier, E., Hock, R., Pfeffer, W. T., Kaser, G., Ligtenberg, S. R. M., Bolch, T., Sharp, M. J., Hagen, J. O., van den Broeke, M. R., and Paul, F.: A reconciled estimate of glacier contributions to sea level rise: 2003 to 2009, Science, 340, 852–857, 2013.

Goelzer, H., Huybrechts, P., Fürst, J. J., Nick, F. M., Andersen, M. L., Edwards, T. L., Fettweis, X., Payne, A. J., and Shannon, S.: Sensitivity of Greenland ice sheet projections to model formulations, J. Glaciol., 59, 733–749, doi:10.3189/2013JoG12J182, 2013.

Hagen, J. O., Liestøl, O., Roland, E., and Jørgensen., T.: Glacier Atlas of Svalbard and Jan Mayen, Norwegian Polar Institue, Oslo, 1993.

Isaksen, K., Benestad, R. E., Harris, C., and Sollid, J. L.: Recent extreme near-surface permafrost temperatures on Svalbard in relation to future climate scenarios, Geophys. Res. Lett., 34, L17502, doi:http://dx.doi.org/10.1029/2007GL03100210.1029/2007GL031002, 2007.

Kaser, G., Cogley, J. G., Dyurgerov, M. B., Meier, M. F., and Ohmura, A.: Mass balance of glaciers and ice caps: consensus estimates for 1961–2004, Geophys. Res. Lett., 33, L19501, doi:http://dx.doi.org/10.1029/2006GL02751110.1029/2006GL027511, 2006.

Lang, C., Fettweis, X., and Erpicum, M.: Stable climate and surface mass balance in Svalbard over 1979–2013 despite the Arctic warming, The Cryosphere, 9, 83–101, doi:10.5194/tc-9-83-2015, 2015.

Lenaerts, J. T. M., van Angelen, J. H., van den Broeke, M. R., Gardner, A. S., Wouters, B., and van Meijgaard, E.: Irreversible mass loss of Canadian Arctic Archipelago glaciers, Geophys. Res. Lett., 40, 870–874, doi:http://dx.doi.org/10.1002/grl.5021410.1002/grl.50214, 2013.

Marzeion, B., Jarosch, A. H., and Hofer, M.: Past and future sea-level change from the surface mass balance of glaciers, The Cryosphere, 6, 1295–1322, doi:http://dx.doi.org/10.5194/tc-6-1295-201210.5194/tc-6-1295-2012, 2012.

Meehl, G. A., Stocker, T. F., Collins, W. D., Friedlingstein, P., Gaye, A. T., Gregory, J. M., Kitoh, A., Knutti, R., Murphy, J. M., Noda, A., Raper, S. C. B., Watterson, I. G., Weaver, A. J., and Zhao, Z.-C.: Global climate projections, in: Climate Change 2007: The Physical Science Basis. Contribution of Working Group I to the Fourth Assessment Report of the Intergovernmental Panel on Climate Change, edited by: Solomon, S., Qin, D., Manning, M., Chen, Z., Marquis, M., Averyt, K. B., Tignor, M., and Miller, H. L., Cambridge University Press, Cambridge, UK and New York, NY, USA, 2007.

Meier, M. F., Dyurgerov, M. B., Rick, U. K., O'Neel, S., Pfeffer, W. T., Anderson, R. S., Anderson, S. P., and Glazovsky, A. F.: Glaciers dominate eustatic sea-level rise in the 21st century, Science, 317, 1064–1067, 2007.

Moss, R. H., Edmonds, J. A., Hibbard, K. A., Manning, M. R., Rose, S. K., van Vuuren, D. P., Carter, T. R., Emori, S., Kainuma, M., Kram, T., Meehl, G. A., Mitchell, J. F. B., Nakicenovic, N., Riahi, K., Smith, S. J., Stouffer, R. J., Thomson, A. M., Weyant, J. P., and Wilbanks, T. J.: The next generation of scenarios for climate change research and assessment, Nature, 463, 747–756, 2010.

Noël, B., Fettweis, X., van de Berg, W. J., van den Broeke, M. R., and Erpicum, M.: Sensitivity of Greenland Ice Sheet surface mass balance to perturbations in sea surface temperature and sea ice cover: a study with the regional climate model MAR, The Cryosphere, 8, 1871–1883, doi:http://dx.doi.org/10.5194/tc-8-1871-201410.5194/tc-8-1871-2014, 2014.

Radić, V. and Hock, R.: Regionally differentiated contribution of mountain glaciers and ice caps to future sea-level rise, Nat. Geosci., 4, 91–94, doi:http://dx.doi.org/10.1038/ngeo105210.1038/ngeo1052, 2011.

Radić, V., Bliss, A., Beedlow, A. C., Hock, R., Miles, E., and Cogley, J. G.: Regional and global projections of twenty-first century glacier mass changes in response to climate scenarios from global climate models, Clim. Dynam., 42, 37–58, doi:http://dx.doi.org/10.1007/s00382-013-1719-710.1007/s00382-013-1719-7, 2014.

Rignot, E., Velicogna, I., van den Broeke, M. R., Monaghan, A., and Lenaerts, J. T. M.: Acceleration of the contribution of the Greenland and Antarctic ice sheets to sea level rise, Geophys. Res. Lett., 38, L05503, doi:http://dx.doi.org/10.1029/2011GL04658310.1029/2011GL046583, 2011.

Rignot, E., Mouginot, J., Morlighem, M., Seroussi, H., and Scheuchl, B.: Widespread, rapid grounding line retreat of Pine Island, Thwaites, Smith, and Kohler glaciers, West Antarctica, from 1992 to 2011, Geophys. Res. Lett., 41, 3502–3509, doi:http://dx.doi.org/10.1002/2014GL06014010.1002/2014GL060140, 2014.

Rogelj, J., Meinshausen, M., and Knutti, R.: Global warming under old and new scenarios using IPCC climate sensitivity range estimates, Nat. Clim. Change, 2, 248–253, doi:http://dx.doi.org/10.1038/nclimate138510.1038/nclimate1385, 2012.

Sakamoto, T. T., Komuro, Y., Nishimura, T., Ishii, M., Tatebe, H., Shiogama, H., Hasegawa, A., Toyoda, T., Mori, M., Suzuki, T., Imada, Y., Nozawa, T., Takata, K., Mochizuki, T., Ogochi, K., Emori, S., Hasumi, H., and Kimoto, M.: MIROC4h – a new high-resolution atmosphere–ocean coupled general circulation model, J. Meteorol. Soc. Jpn., 90, 325–359, doi:http://dx.doi.org/10.2151/jmsj.2012-30110.2151/jmsj.2012-301, 2012.

Shepherd, A., Ivins, E. R., A, G., Barletta, V. R., Bentley, M. J., Bettadpur, S., Briggs, K. H., Bromwich, D. H., Forsberg, R., Galin, N., Horwath, M., Jacobs, S., Joughin, I., King, M. A., Lenaerts, J. T. M., Li, J., Ligtenberg, S. R. M., Luckman, A.,

Luthcke, S. B., McMillan, M., Meister, R., Milne, G., Mouginot, J., Muir, A., Nicolas, J. P., Paden, J., Payne, A. J., Pritchard, H., Rignot, E., Rott, H., Sørensen, L. S., Scambos, T. A., Scheuchl, B., Schrama, E. J. O., Smith, B., Sundal, A. V., van Angelen, J. H., van de Berg, W. J., van den Broeke, M. R., Vaughan, D. G., Velicogna, I., Wahr, J., Whitehouse, P. L., Wingham, D. J., Yi, D., Young, D., and Zwally, H. J.: A reconciled estimate of of ice-sheet mass balance, Science, 338, 1183–1189, 2012.

van Angelen, J. H., Lenaerts, J. T. M., van den Broeke, M. R., Fettweis, X., and van Meijgaard, E.: Rapid loss of firn pore space accelerates 21st century Greenland mass loss: Geophys. Res. Lett., 40, 1–5, doi:10.1002/grl.50490, 2013.

Watanabe, M., Suzuki, T., O'ishi R., Komuro, Y., Watanabe, S., Emori, S., Takemura, T., Chikira, M., Ogura, T., Sekiguchi, M., Takata, K., Yamazaki, D., Yokohata, T., Nozawa, T., Hasumi, H., Tatebe, H., and Kimoto, M.: Improved climate simulation by MIROC5: mean states, variability, and climate sensitivity, J. Climate, 23, 6312–6335, 2010.

Zuo, Z., and Oerlemans, J.: Modelling albedo and specific balance of the Greenland ice sheet: calculations for the Søndre Strømfjord transect, J. Glaciol., 42, 305–317, 1996.

Table 1. Anomaly of the the energy balance components ($\mathrm{W\,m^{-2}}$) and relative contribution of the energy balance components to the NET anomaly (2080–2099 mean compared to the historical period).
table

E balance component	Anomaly ($\mathrm{W\,m^{-2}}$)	% of NET anomaly
SWnet	25	33
SWDalb	38	49
SWDswd	-6	-7.5
SHF	19	24
LHF	17	22
LWnet	16	21
NET	77	

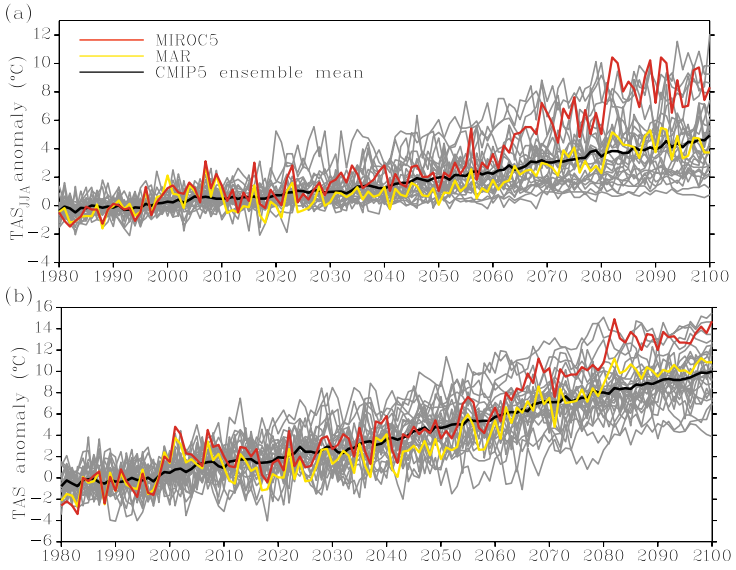

Fig. 1. (a) 1980–2100 evolution of the JJA near-surface temperature (TAS_{JJA}, °C) anomaly over Svalbard with respect to the 1980–2005 mean simulated by MIROC5 (red curve), the CMIP5 GCMs (grey curves), the ensemble mean (black curve) and MAR forced by MIROC5 under the RCP8.5 scenario (yellow curve). **(b)** Same as **(a)** but for the annual near-surface temperature.
figure

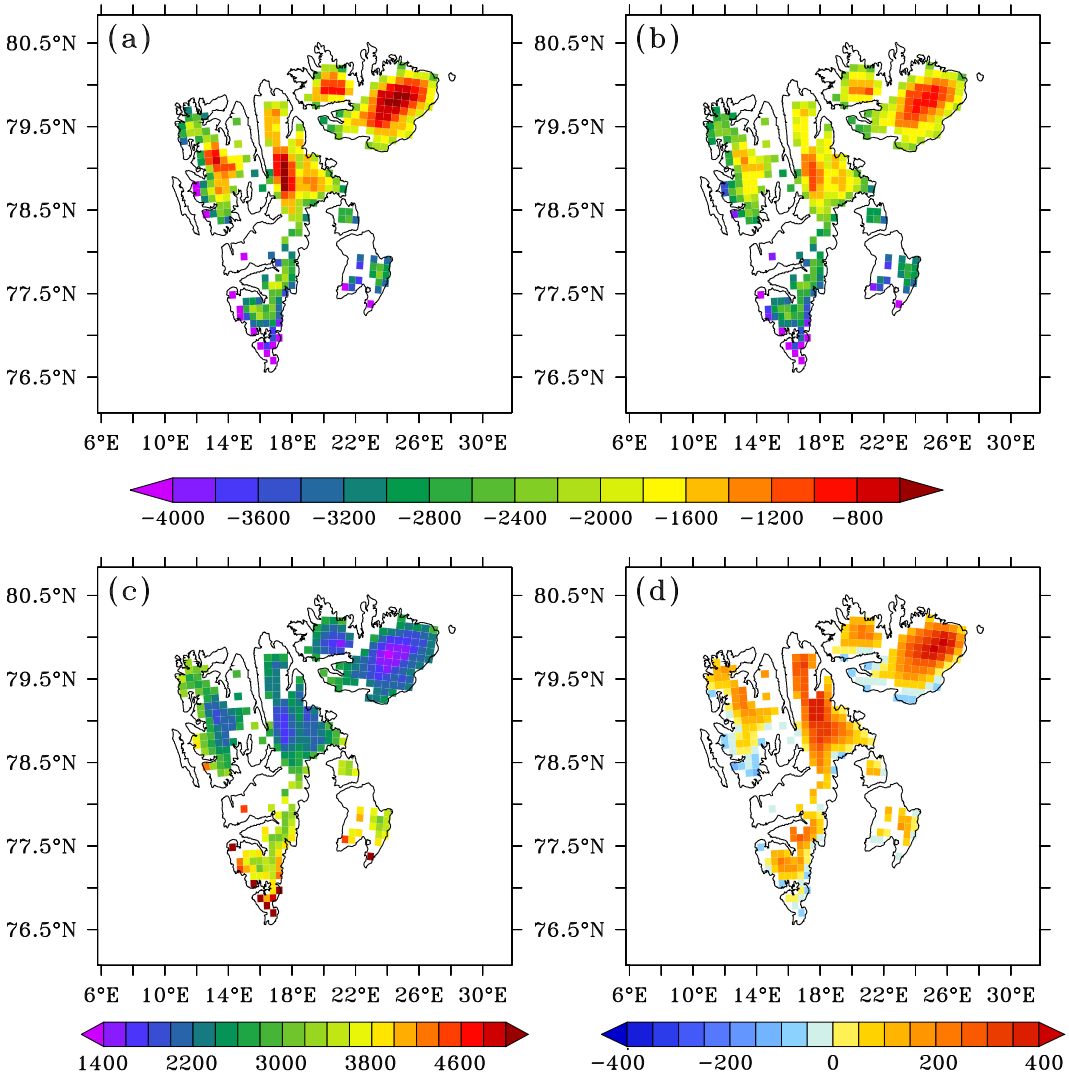

Fig. 2. (a) 2070–2099 mean SMB ($\mathrm{mm\,w.e.\,yr^{-1}}$) as simulated by MAR forced by the MIROC5-based RCP8.5 scenario. **(b)** Difference between **(a)** and the 1980–2005 mean shown in Fig. 14 in Lang et al. (2015). **(c)** Same as **(b)** but for runoff. **(d)** Same as **(b)** but for precipitation.

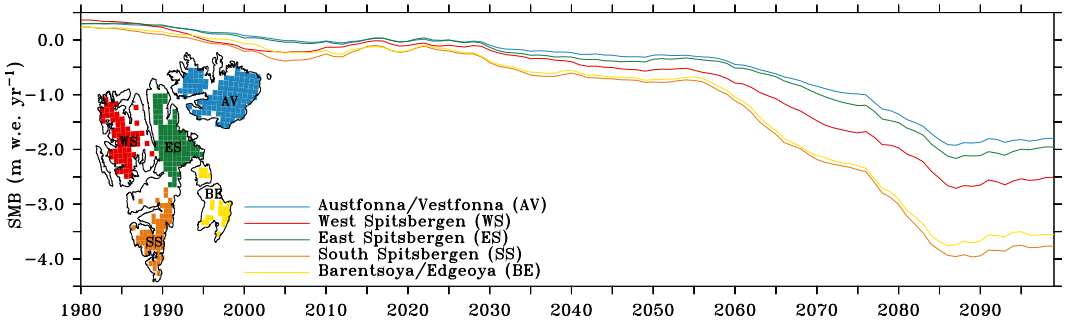

Fig. 3. SMB 10-year running mean ($\mathrm{m\,w.e.\,yr^{-1}}$) for 5 different regions (Austfonna and Vestfonna, west Spitsbergen, east Spitsbergen, south Spitsbergen and Barentsøya and Edgeøya) as simulated by MAR forced by the MIROC5-based historical scenario over 1980–2005 and RCP8.5 afterwards. The units are in $\mathrm{m\,w.e.\,yr^{-1}}$ (rather than $\mathrm{Gt\,yr^{-1}}$) to be independent of different region areas. The permanent ice mask of each region defined for the regional evolution is shown in the inset.

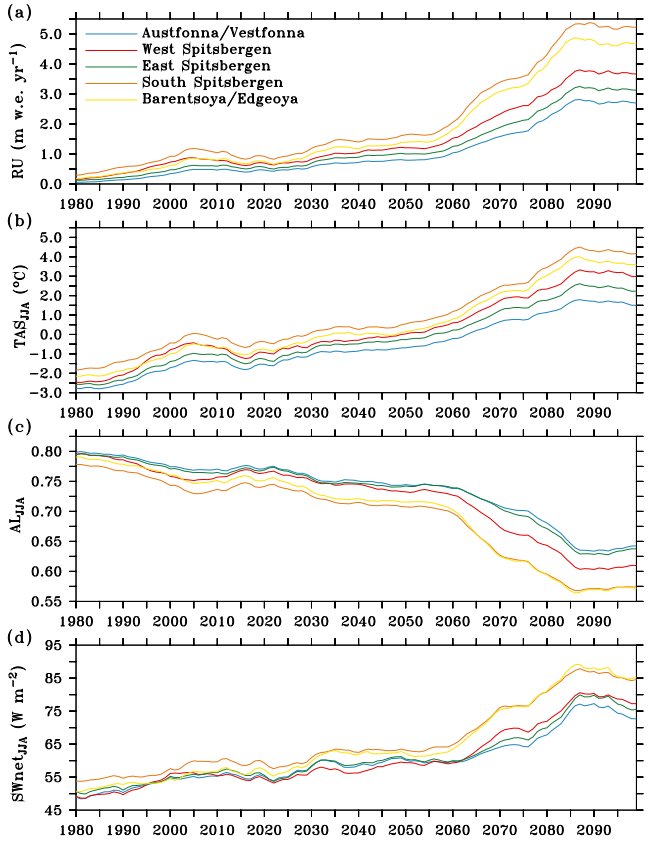

Fig. 4. **(a)** 10-year running mean of the meltwater runoff (RU, $\mathrm{m\,w.e.\,yr^{-1}}$) over 1980–2099 for the 5 regions shown in Fig. 3. **(b)** Same as **(a)** but for the near-surface JJA temperature ($\mathrm{TAS_{JJA}}$, $^{\circ}\mathrm{C}$) **(c)** Same as **(a)** but for the JJA albedo ($\mathrm{AL_{JJA}}$). **(d)** Same as **(a)** but for the JJA net solar radiation absorbed by the surface ($\mathrm{SWnet_{JJA}}$,$\mathrm{W\,m^{-2}}$).

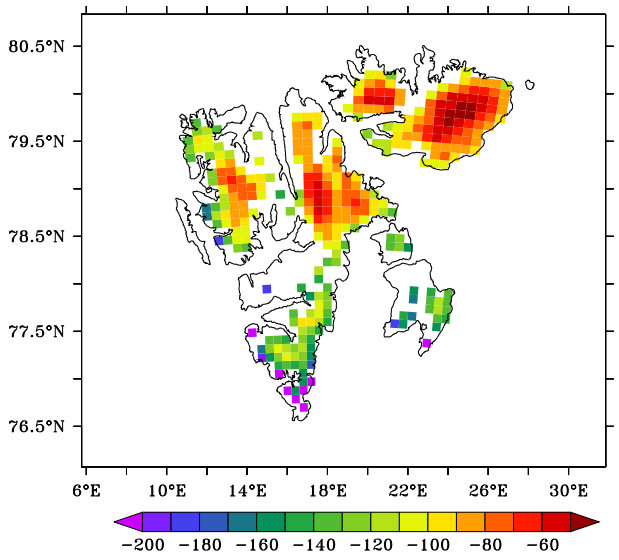

Fig. 5. Projected cumulated anomaly of the SMB changes (m w.e.) over the 21st century. The SMB anomaly is the difference with the 1980–2005 mean and has been summed over 2000–2100.

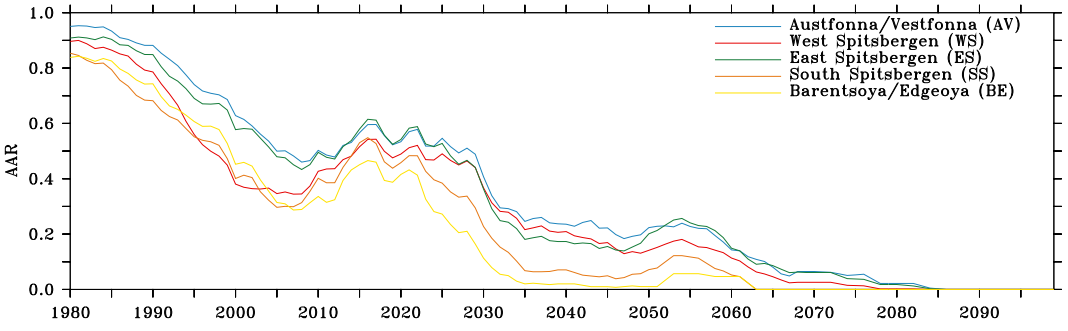

Fig. 6. 10-year running mean of the accumulation area ratio (AAR) over 1980–2099 for the 5 regions shown in Fig. 3. AAR represents the ratio of the area of the accumulation zone of a region compared to the total area of the region, i.e. the proportion of a region that is in the accumulation area.

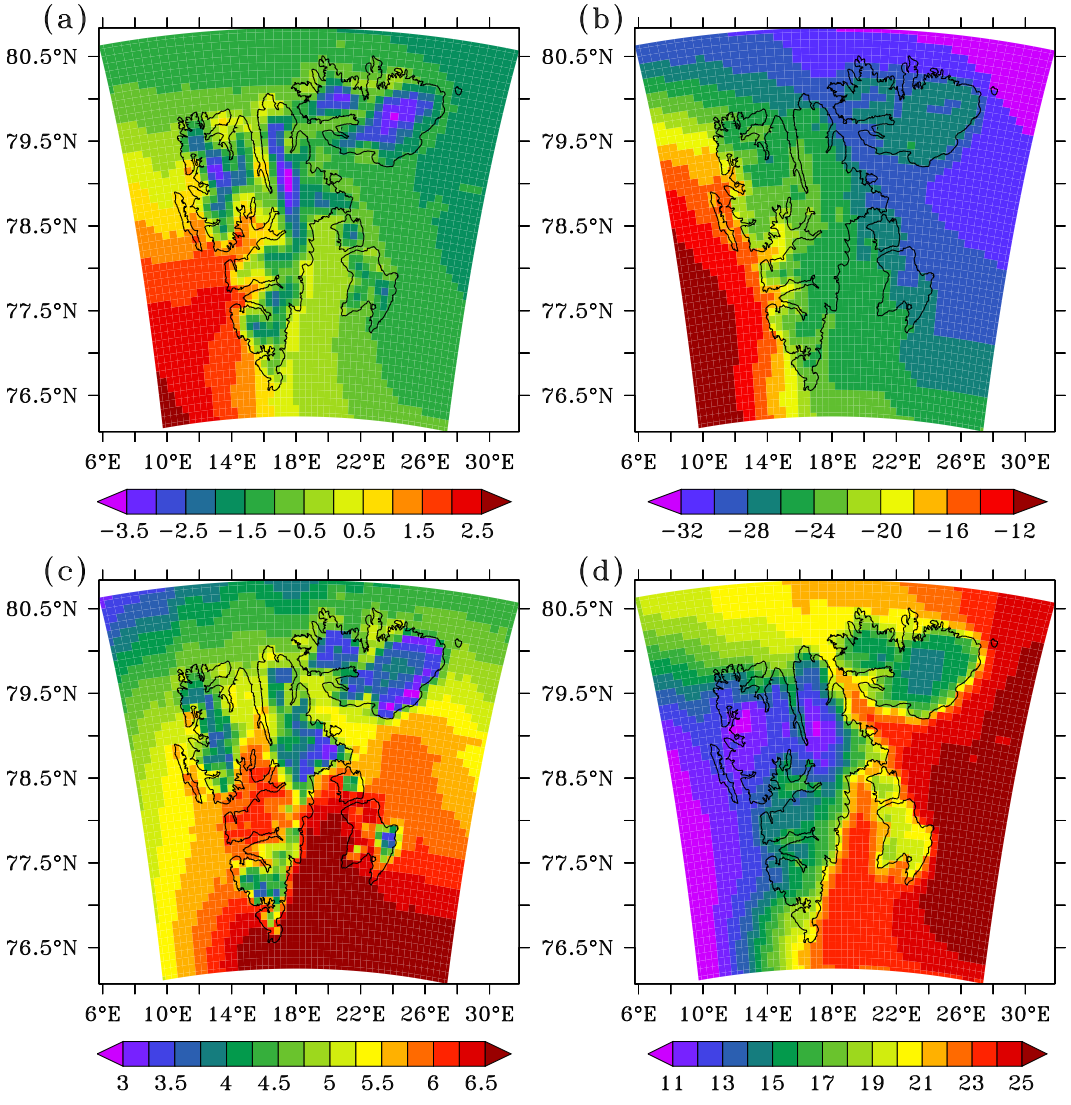

Fig. 7. (a) 1980–2005 mean summer (JJA) near-surface temperature (°C). **(b)** Same as **(a)** but for winter (DJF). **(c)** 2070–2099 mean summer (JJA) near-surface temperature anomaly (°C) with respect to the 1980–2005 mean. **(d)** Same as **(c)** but for winter (DJF).

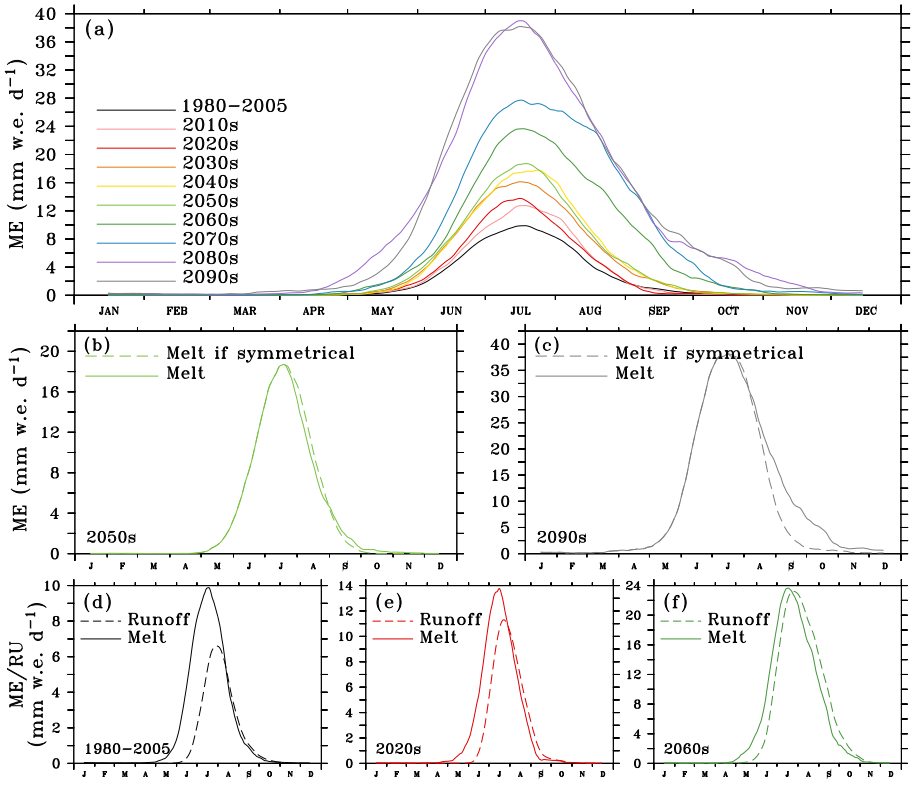

Fig. 8. **(a)** Mean annual cycle of the surface melt (mm w.e. d^{-1}, 30-day running mean) for the listed decades. The 1980–2005 mean is shown in black as comparison. **(b)** Annual cycle of the surface melt in the 2050s (solid line) as well as, in dash, the cycle if it was symmetrical with respect to its maximum. **(c)** Same as **(b)** but for the 2090s. **(d)** Mean annual cycle of the melt (solid line) and runoff (dashed line) (mm w.e. d^{-1}) during the 1980–2005 period. **(e)** Same as **(d)** in the 2020s. **(f)** Same as **(d)** in the 2060s.

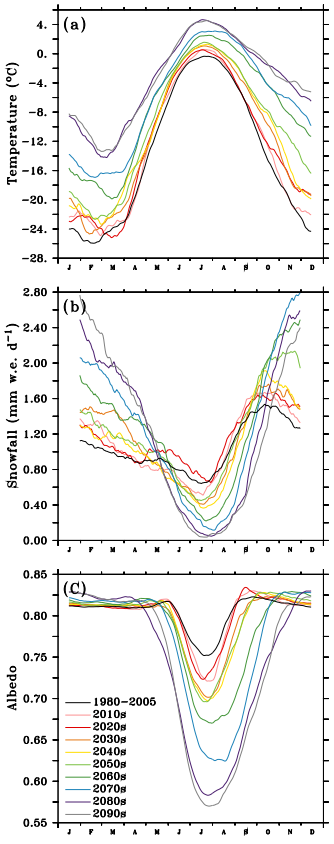

Fig. 9. (a) Mean annual cycle of TAS ($^{\circ}$C, 30-day running mean) over the permanent ice covered area for the listed decades. The 1980–2005 mean is given in black as comparison. **(b)** Same as **(a)** but for the snowfall ($\mathrm{mm\,w.e.\,d^{-1}}$). As the daily variability of precipitation is very high, we have applied here a 60-day running mean instead of 30 days (like in Figs. 8 and 9a and c) in order to make the figure more clear. **(c)** Same as **(a)** but for the albedo.

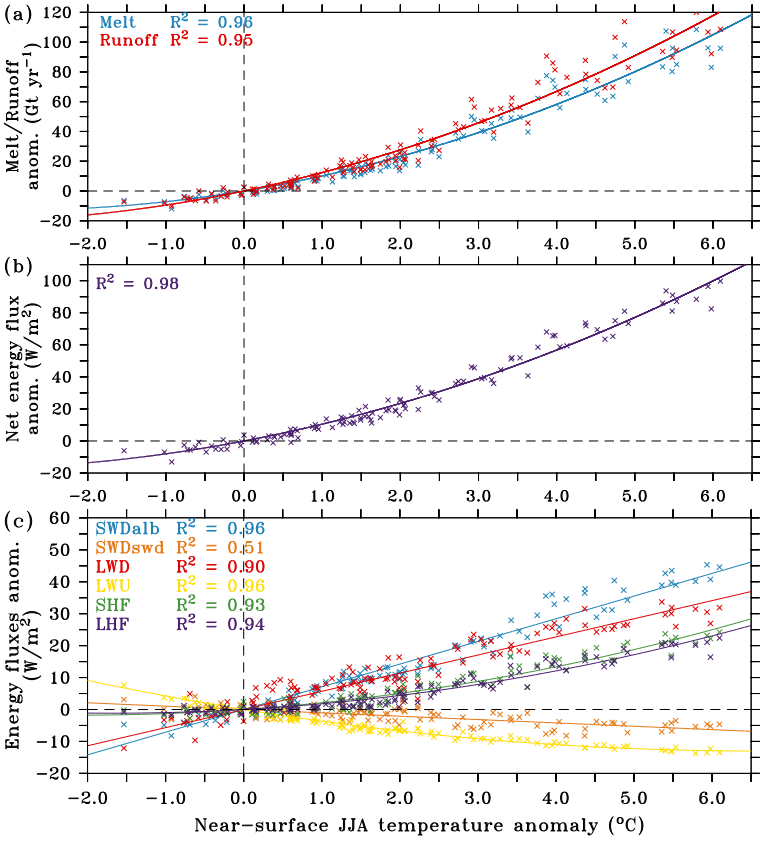

Fig. 10. **(a)** Melt and runoff anomalies ($\mathrm{Gt\,yr^{-1}}$) vs. $\mathrm{TAS_{JJA}}$ anomaly ($^{\circ}\mathrm{C}$). The anomalies are differences with respect to the 1980–2005 mean. **(b)** Same as **(a)** but for the JJA net energy flux at the surface ($\mathrm{W\,m^{-2}}$). **(c)** Same as **(b)** but for the JJA energy balance components. The solid lines are quadratic regression curves.